Title

Three-Dimensionally Aligned Sulfur Electrodes by Directional Freeze Tape Casting

Journal

Nano Letters, 19(7)

ISSN

1530-6984

Authors

Hwa, Yoon

Yi, Eongyu

Shen, Hao

et al.

Publication Date

2019-07-10

DOI

10.1021/acs.nanolett.9b01805

Peer reviewed

Three-dimensionally aligned sulfur electrodes by directional freeze tape casting

Yoon Hwa,[a,b,‡] Eongyu Yi,[a,‡] Hao Shen,[c,d] Younghoon Sung,[b] Jiawei Kou,[d] Kai Chen,[d] Dilworth Y. Parkinson,[c] Marca M. Doeff[a,] and Elton J. Cairns[a,b,*]*

a Energy Storage and Distributed Resources Division, Lawrence Berkeley National Laboratory, Berkeley, California, 94720, USA

b Department of Chemical and Biomolecular Engineering, University of California, Berkeley, California, 94720, USA

c Advanced Light Source, Lawrence Berkeley National Laboratory, Berkeley, California, 94720, USA

d Center for Advancing Materials Performance from the Nanoscale (CAMP-Nano), State Key Laboratory for Mechanical Behavior of Materials, Xi'an Jiaotong University, Xi'an, Shaanxi 710049, China

ABSTRACT

Rational design of sulfur electrodes is exceptionally important in enabling a high performance lithium/sulfur cell. Constructing a continuous pore structure of the sulfur electrode that enables facile lithium ion transport into the electrode and mitigates the reconstruction of sulfur is a key factor for enhancing the electrochemical performance. Here, we report a three-dimensionally (3D) aligned sulfur electrode cast onto conventional aluminium foil by directional freeze tape casting. The 3D aligned sulfur-graphene oxide (S-GO) electrode consisting of a few micron-thick S-GO layers with 10-20 μm interlayer spacings demonstrates significant improvement in the performance of the Li/S cell. Moreover, the freeze tape cast graphene oxide electrode exhibits homogenous reconfiguration behaviour in the polysulfide catholyte cell tests, and demonstrated extended cycling capability with only 4 % decay of the specific capacity over 200 cycles. This work emphasizes the critical importance of proper structural design for sulfur-carbonaceous composite electrodes.

KEYWORDS: Li/S cells; Freeze tape casting; Porous electrode; Three-dimensional pore alignment

TEXT

The continued development of electrochemical energy storage and conversion systems (e.g. batteries, fuel cells and supercapacitors) has made a tremendous impact on the infrastructure of modern society. Rechargeable batteries, as represented by lithium ion cells, have been adopted in numerous electronic devices such as cell phones, laptops, smart pads, and various household

electronics, making it difficult to imagine a world without them. Recently, the field of rechargeable battery applications is expanding to include vehicle electrification, which requires advanced battery systems offering high specific energy (> 300 Wh/kg) at an affordable cost and with improved safety. However, such requirements are unlikely to be met using conventional lithium ion cells.

To satisfy the demands of the emerging markets for advanced battery systems, researchers have explored several alternative systems. Among them, the Li/S cell has gained great attention from the battery community owing to its very high theoretical specific energy (2600 Wh/kg) and promising potential to lower the battery price.[1-4] However, there were many challenges in developing the Li/S cell chemistry. For example, the low electrical conductivity of sulfur (and Li_2S), polysulfide shuttling,[4-7] and instability of the lithium electrode at high sulfur mass loading are well known issues.

Tangible progress in improving the performance of Li/S cells has been made in the last several years.[8-18] One of the key strategies to develop high specific energy Li/S cells is to rationally design porous sulfur electrodes such that efficient electronic and ionic pathways are provided to the active sulfur throughout the thickness of the electrode. Such a design promotes the reaction kinetics of active sulfur, resulting in improved sulfur utilization, essential for higher practical specific energy. In addition, structural reconfiguration of the sulfur electrode occurs during cell operation as sulfur repeatedly dissolves and redeposits in the positive electrode, which can impede the rate capability of the Li/S cell if significant accumulation of sulfur (or Li_2S) forms at the sulfur electrode surface. Because the reconfiguration behaviour strongly depends on the original architecture of the electrode, one of the successful approaches that addresses this issue is the use of highly porous foam-structured current collectors[8-11] which, however, come with

technical issues associated with the manufacturing of the sulfur electrodes including difficult tabbing for terminal connections, difficult slurry casting, and high implementation costs.

To overcome the above-listed shortcomings of using foam current collectors and reap the benefits of controlled pore structures, we use freeze tape casting, a combination of conventional freeze casting[19, 20] and tape casting. Freeze casting is the method for templating of porous structures by the water frozen, which is particularly used for creating the unique porous structure of ceramics.[20] In conventional freeze casting, the slurry is poured into a mold placed on a cooling plate, which either cools down below the solvent freezing temperature after the slurry is introduced or is pre-cooled to a target temperature. The ice nucleates and grows along the thermal gradient, which leaves behind low-tortuosity open pore channels after sublimation of the ice, during the later steps of the freeze drying process. Previously, freeze casting was used for the graphite[21] and lithium nickel cobalt aluminum oxide electrodes[22] and the freeze cast electrodes exhibited promising power capability due to its low-tortuosity, however, the developed electrodes were ceramic monoliths which requires additional effort for engaging with an appropriate current collector.

In the freeze tape casting process (Scheme 1), the modified freeze casting method,[23] two-directional thermal gradients are imposed upon the tape casting slurry: one from the freezing plate to the top of the slurry; another resulting from the directional movement of the tape cast slurry, which results in the 3D aligned freezing of the water. Especially, conventional slurry composition consisting of active material, carbon additive and polymer binder was directly cast onto conventional aluminium (Al) foil current collector, so that no additional step is required for attaching the electrode onto current collector, which is significant difference from earlier works. After removing the ice template, a 3D array of the electrode components with vertical open pore

channels (which are filled with liquid electrolyte during cell assembly) is constructed. The freeze tape casting process does not involve any chemical reactions, thus no by-product removal step is required. It is also environmentally benign as water is used as the solvent. Recently, a freeze tape cast $Li_4Ti_5O_{12}$ electrode for conventional lithium ion cells was shown to have superior rate capability compared to that of a conventional tape cast electrode.[24] The freeze tape cast sulfur electrodes in this work also showed superior electrochemical properties compared to the control. Sulfur electrodes with vertically aligned open channels constructed onto a conventional Al foil current collector were produced using this method. The directional, low-tortuosity, externally accessible channels, which run parallel to the ion diffusion direction during cycling, is a key design factor, as they provide a conduction highway to overcome rate limitations, in contrast to a randomly oriented pore structure.[25-27]

To evaluate the freeze tape cast sulfur electrode, a cetyltrimethylammonium bromide (CTAB) modified sulfur-graphene oxide (S-GO-CTA) nanocomposite[10,28] consisting of thin graphene oxide (GO) flake-like particles and unagglomerated sulfur was synthesized as shown in Figure S1 (scanning electron microscopy image, SEM). It was determined to have a sulfur content of 75 % by thermogravimetric analysis (TGA, Figure S2). The freeze tape casting was conducted using an aqueous slurry composed of the S-GO-CTA composite as active material, Ketjen black, and carbon nanotubes (CNTs) as conducting additives, and a composite binder (styrene butadiene rubber (SBR) and carboxymethyl cellulose (CMC)) with a controlled thickness of 300 μm (FTC-300) or 200 μm (FTC-200). The top view (Figure 1a) and the cross-sectional view (Figure 1b) SEM images of the FTC-300 electrode show a rather uniform interlayer spacing (Figure 1e). Figure 1d shows that the S-GO-CTA layers are a few microns thick with Ketjen black particles and CNTs homogeneously distributed on the surface of the S-GO-CTA composite (Figure 1c).

The externally accessible and aligned laminar pore structure of FTC-300 is clearly observed using volume rendering micro computed tomography (micro CT) as shown in Figure 1d, obtained on beamline 8.3.2 at the Advanced Light Source (ALS, Lawrence Berkeley National Laboratory in the United States). In the interlayer spacing calculation results (Figure 1e) obtained from the Fourier transform pattern (Figure S3), a very uniform interlayer spacing of 10-20 μm throughout the whole electrode thickness is observed, implying a low tortuosity of the pores in the FTC-300 electrode. The FTC-200 electrode also exhibits a uniformly 3D aligned pore architecture as shown in SEM images (Figure S4a and S4b) and volume rendering image (Figure S4c). By controlling the electrode thickness, different sulfur areal mass loadings of ~2.0 mgS/cm^2 and ~3.6 mgS/cm^2 were obtained for the FTC-200 and the FTC-300 electrodes, respectively.

To verify that the 3D aligned pore structure provides enhanced cell performance, the FTC-200 electrode was galvanostatically cycled at several different current densities in a Type 2032 coin cell with a Li foil counter electrode. As a control, a tape cast S-GO-CTA electrode (TC electrode, ~1.7 mgS/cm^2) was also prepared using the same batch of the slurry (SEM image is shown in Figure S5) and tested at the same current densities. As shown in Figure 2a, the FTC-200 electrode delivers a discharge specific capacity of ~1270 mAh/g at 0.1 mA/cm^2 and maintained 707 mAh/gS at 1.0 mA/cm^2. Notably, a capacity drop of only 50 mAh/g relative to that obtained at 1.0 mA/cm^2 was demonstrated at a current density of 3.0 mA/cm^2, which shows the good rate performance of the FTC-200 electrode. In contrast, the TC electrode showed a lower initial specific capacity of 977 mAh g^{-1}S at 0.1 mA/cm^2 and 371 mAh/g^{-1}S at 3.0 mA/cm^2; only 56 % of the specific capacity relative to that of the FTC-200 electrode measured at the same current density. Moreover, the specific capacity of the TC electrode gradually decreased at each current density, whereas the FTC-200 electrode retained its specific capacity.

Cyclic voltammetry test results (CV, Figure 2b) correspond to the rate performance test results; the FTC-200 electrode exhibited sharper and smaller redox peak shifts compared to those of the TC electrode at a sweep rate of 0.1 mV/s, indicating the better rate capability of the FTC-200 electrode. Since both electrodes were prepared with the same batch of slurry, the major difference between the FTC-200 and the TC electrode is solely the pore structure. Thus, it can be hypothesized that the better rate performance of the FTC-200 electrode is attributed to the very accessible, open and continuously 3D aligned pore structure. This structure provides lithium ions with a more facile pathway to the active sulfur, so that the rate performance of the Li/S cell is enhanced. The electrochemical impedance spectroscopy results shown in Figure 2c support this hypothesis, where the FTC-200 electrode obviously shows a smaller cell impedance than the TC electrode.

In addition, the wide interlayer spacing with low tortuosity of the freeze tape cast electrode is beneficial for stabilizing the sulfur electrode. In general, the solution-based reaction chemistry, which involves formation of soluble lithium polysulfide intermediates and re-deposition as Li_2S (or sulfur) continuously occurs during cell operation and changes the electrode structure during cell operation. If the Li_2S (or sulfur) forms a deposit that blocks the electronic or ionic pathways of the electrode due to high tortuosity or by obstructing the entrance of the pores of the electrode, significant cell impedance will develop, which results in cell performance degradation.[3] In the case of the freeze tape cast electrodes, however, the wide interlayer spacing with low tortuosity avoids the blocking of the electrical pathway by Li_2S deposits, so that a more stable reconfiguration of the electrode can be achieved. Reflecting these advantages, the FTC-200 electrode demonstrates improved cycling behaviour over 250 cycles (Figure 2d) with no significant overpotential development at each different current density (Figure S6). Even at a

higher sulfur loading of 3.6 mg/cm^2 (FTC-300 electrode), excellent rate performance was still obtainable, where the specific capacity of about ~ 740 mAh g^{-1}S was demonstrated at 2.0 mA/cm^2 (Figure 2e), corresponding to a 1.2 h discharge rate, while maintaining the prolonged second discharge plateau around 2.1 V (Figure 2f). Since the coin cell assembly process provides compression to the electrode which may cause damage to the unique electrode structure, it is worthwhile investigating the electrode structure after cell assembly. As shown in Figure S7, the 3D aligned pore structure the FTC-300 electrode collected from the coin cell was preserved, while the thickness of the FTC-300 electrode was reduced to 180 μm (60 % relative to its original thickness). Thus, it can be concluded that the 3D aligned pore structure maintains its unique structure under the pressure given by the coin cell parts and improve the rate performance of the Li/S cells.

To further verify the architectural effect of the freeze tape cast electrodes, polysulfide catholyte cell tests were conducted with a freeze tape cast GO electrode (FTC-GO). As a control, a tape cast GO electrode (TC-GO) was also prepared with a slurry composed of freeze-dried GO powder and SBR binder. The GO powder for the TC-GO electrode was prepared *via* freeze drying of a single layered GO suspension so that the highly porous structure of the freeze-dried GO flakes can lead to a good porous structure of the TC-GO electrode. As shown in SEM (Figure 3a) and volume rendering images (Figure S8), the 3D aligned GO framework of the FTC-GO electrode was produced by the freeze tape casting method, while the TC-GO electrode forms a randomly distributed pore structure (SEM, Figure 3b). Cyclic voltammetry was conducted to investigate the electrochemical behaviour of the electrodes (Figure 4a) and it can be easily seen in the CV curves that the FTC-GO electrode shows sharp and distinguishable redox peaks, whereas the TC-GO electrode shows much less well-delineated redox peaks due to large

discharge and charge overpotentials, and less accessible area. These results emphasize that the 3D aligned pore structure is very advantageous to good rate capability involving lithium polysulfide in the catholyte, similar to the electrochemical behaviour of the FTC-200 electrode in the Li/S cells discussed above.

In galvanostatic cycle tests (Figure 4c) of the polysulfide catholyte cells, both the FTC-GO electrode and the TC-GO electrode deliver high specific capacities of 970 and 850 mAh $g^{-1}S$, respectively, at the initial discharge rate of 0.15 mA cm^{-2} of the GO electrode. However, the specific capacity of the TC-GO electrode dropped immediately to 400 mAh/gS, once the rate increased to 0.3 mA/cm^{2} of the GO electrode, whereas the FTC-GO electrode still showed a specific capacity of 805 mAh/gS. Notably, the FTC-GO electrode successfully maintained 96 % of the original specific capacity (relative to the specific capacity obtained at the second cycle) over 200 cycles (Figure 4b). Interestingly, even with the lower utilization of the TC-GO electrode (in other words, less sulfur deposition onto the GO electrode), the top surface of the TC-GO electrode was completely covered by deposited sulfur (or unreacted Li_2S after charging) after the initial discharge and charge processes, and no pores were observable (Figure 3d). In contrast, although the aligned graphene sheets tend to be tilted relative to the original structure due to the compressive pressure given to the FTC-GO electrode during cell assembly, the cycled FTC-GO electrode still maintained its externally accessible pores at the top surface of the electrode, (Figure 3c), so that stable capacity retention of the FTC-GO electrode was achieved. The importance of the porous structure in achieving good catholyte cell performance was further demonstrated by testing a dense GO film electrode (Figure S9) which was prepared by the tape casting method using the same slurry that was used for the FTC-GO electrode. Because of the strong aggregation tendency of GO, a very dense GO film structure was constructed after the

drying process. The dense GO film electrode shows a very low specific capacity of 100 mAh/gS at 0.15 mA/cm^2 for the first cycle and almost negligible capacity of about 10-20 mAh g^{-1}S for the following cycles at 0.3 mA/cm^2 (Figure S10). Because of the dense structure of the GO laminates, polysulfides and lithium ions were not able to reach the internal surfaces of the GO electrode, resulting in very limited sulfur utilization. Considering the fact that all three of these electrodes contain same GO, it is clear that the electrode architecture plays a critical role in obtaining good cell performance.

It cannot be overlooked that the GO in the freeze tape cast S-GO-CTA electrode (or in the GO electrode in the polysulfide catholyte cell) behaves not only as a conductive framework, but also as a sulfur immobilizer,[29] so it is worthwhile investigating the influence of the GO morphology on the immobilization of the sulfur. To do so, we prepared highly porous GO and aggregated GO powders using freeze drying (Figure S11) and vacuum drying methods (Figure S12), respectively, and conducted chemical polysulfide absorption tests by varying the amount of the GO powder added to the test solution. As shown in Figure S13, it is clear that the freeze-dried GO powder efficiently adsorbed polysulfide from the test solution as seen by the disappearance of the dark orange color of the test solution. The color of the test solution for the highly porous GO powder became clearer as the amount of the powder increased. In contrast, the test solution of the vaccum-dried GO powder shows no recognizable color change, indicating poor polysulfide absorptivity limited by its agglomerated structure. Consequently, it can be concluded that the functional GO surface is not efficiently utilized, unless the surface is in sufficient contact with the test solution and exposed to polysulfide. Because of the severe aggregation of the vacuum-dried GO, only the outer surface of the GO aggregates adsorbs polysulfide in the test solution, while most of the internal GO surface is prevented from properly

contacting polysulfide in the test solution. UV-vis test results of the collected polysulfide solutions correspond to the color observation results, indicating that most of the UV-vis peaks associated with polysulfide disappear for the freeze-dried GO powder test solution (Figure S14). In contrast, only a slight decrease of the UV-vis peak intensity was detected for the vacuum-dried GO powder test solutions, indicating poor polysulfide adsorption by the aggregated GO powder. Consequently, the importance of the rational design of the porous structure of the sulfur electrode from the structure of the active material particles to the structure of the electrode itself cannot be overemphasized.

We report a 3D aligned sulfur electrode architecture made by directional freeze tape casting, consisting of few-micron-thick S-GO-CTA layers with 10-20 μm interlayer spacings. It was demonstrated that the 3D aligned pore structure of the freeze tape cast S-GO-CTA electrode provides enhanced rate performance with better capacity retention. It was possible to achieve 250 cycles without significant capacity fading in Li/S cells with freeze tape cast electrodes, with much higher overall utilization than for cells containing conventional tape-cast electrodes. The externally accessible and continuously 3D aligned pore structure provides lithium ions in the electrolyte with effective ionic pathways to penetrate the thick sulfur electrode. The 3D aligned pore structure is also effective at mitigating the reconfiguration of the sulfur electrode during cell cycling, which accounts for the good cycling performance. FTC-GO electrodes also exhibit homogenous reconfiguration behavior in the polysulfide catholyte cell tests, and demonstrated extended cycling capability with only 4 % decay of the specific capacity over 200 cycles. Freeze tape casting has been demonstrated to dramatically improve cell performance for both conventional Li/S cells and lithium polysulfide catholyte cells. We believe that this work

emphasizes a critical message regarding the need for proper structural design of sulfur electrodes.

FIGURES

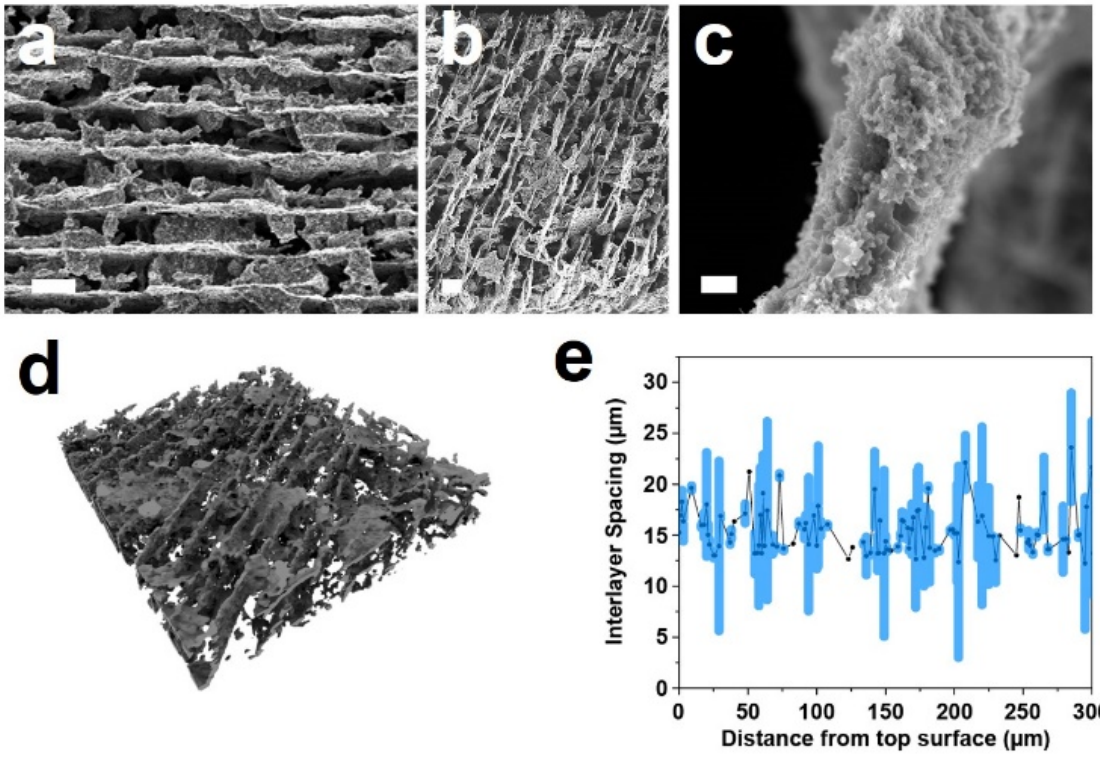

Figure 1. Freeze tape cast S-GO-CTA electrodes. (a-c) SEM images of the FTC-300 electrode. (a) Top view and (b) cross-section view. (Scale bar: 20 μm) and (c) single S-GO-CTA layer of the FTC-300 electrode. (Scale bar: 500 nm). (d) Volume rendering image of the FTC-300 electrode; subvolume size: 490 × 620 × 120 μm (e) Interlayer spacing analysis results for the FTC-300 electrode.

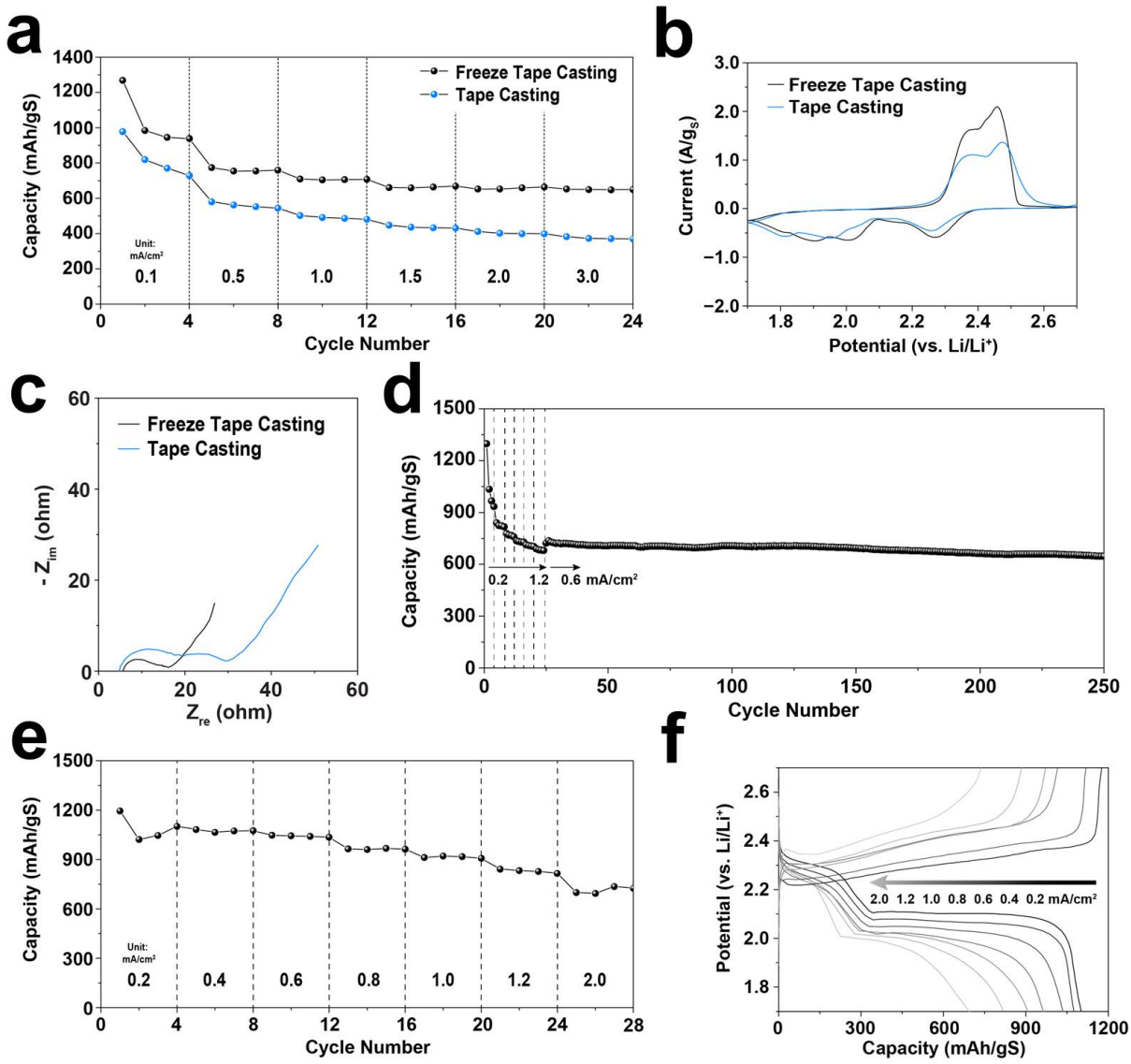

Figure 2. Electrochemical test results. (a-c) Electrochemical test results comparisons of the FTC-200 and conventional TC electrodes. (a) Rate capability at given current densities and (b) cyclic voltammograms obtained at 0.1 mV/s. (sulfur loading: ~ 1.7 mg/cm^2, E/S ratio: 14). (c) Nyquist plot of the FTC-200 and the TC electrode measured at frequencies from 1 MHz to 10 mHz in the fully charged state. (d) Cycling performance at 0.2, 0.4, 0.6, 0.8, 1.0 and 1.2 mA/cm^2 for 4 cycles at each current density, followed by cycling at 0.6 mA/cm^2 (sulfur loading: ~ 2.0 mg/cm^2, E/S ratio: 12) for the FTC-200 electrode. (e-f) Electrochemical test results comparisons of the FTC-

300 electrode. (e) Rate capability and (f) voltage profiles of the FTC-300 electrode at 0.2, 0.4, 0.6, 0.8, 1.0, 1.2 and 2.0 mA/cm^2 for 4 cycles at each current density (sulfur loading: 3.6 mgS/cm^2, E/S ratio: 6.6). The electrolyte was composed of 1.0 M LiTFSI in DOL/DME (1:1, *v*/*v*) with 0.1 M $LiNO_3$.

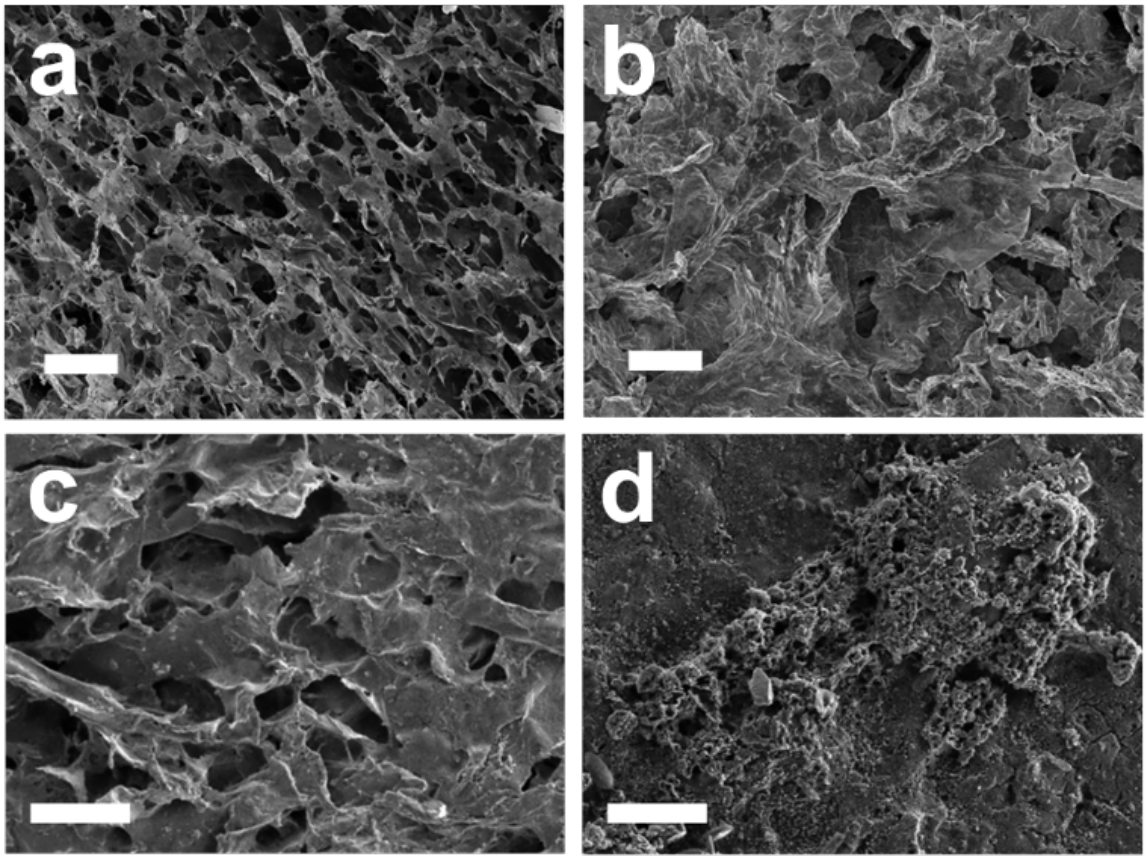

Figure 3. SEM images of the freeze tape cast GO electrode. (a) the pristine FTC-GO and (b) the pristine TC-GO electrodes. SEM images of (c) the FTC-GO and (d) the TC-GO electrodes cycled in the polysulfide catholyte cells. (Scale bar: 20 μm)

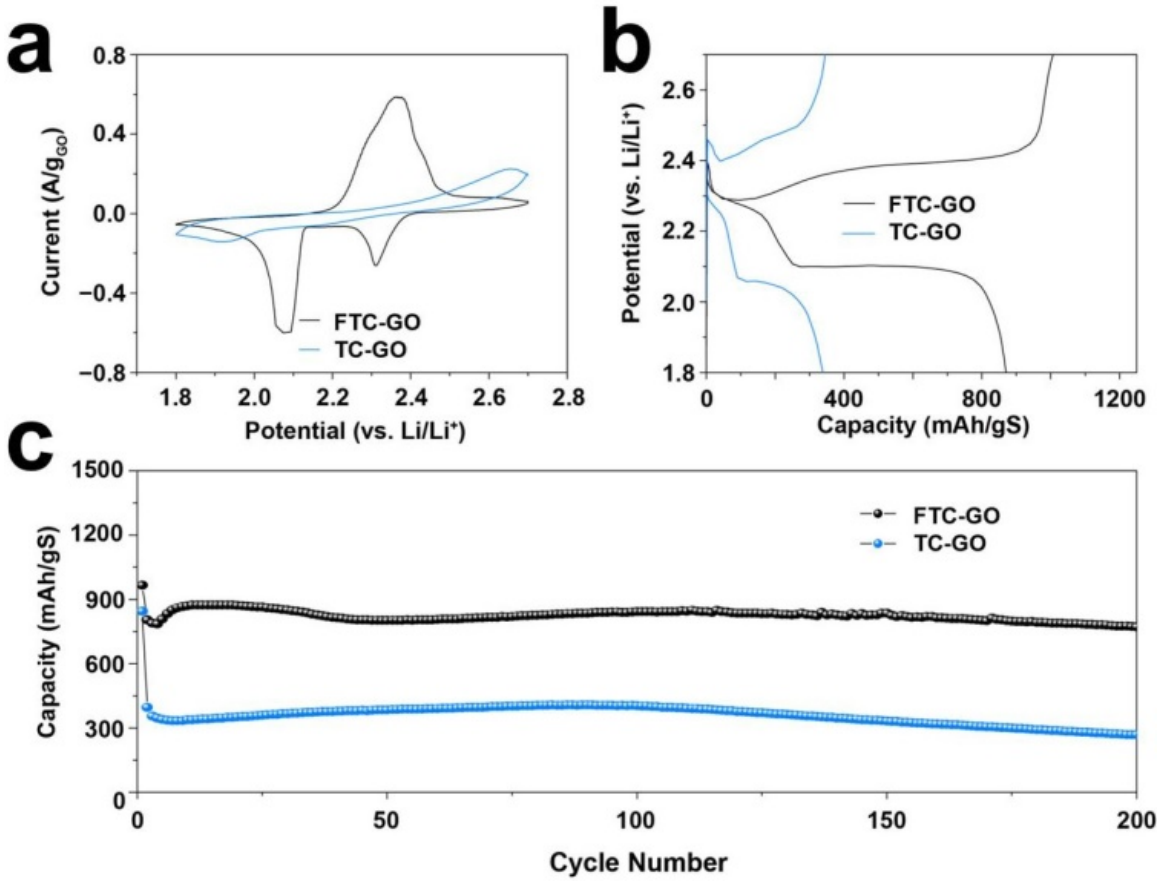

Figure 4. Polysulfide catholyte cell test. (a) CV curves of the FTC-GO and the TC-GO electrodes at a scan rate of 5 μV/s. (b) Voltage profiles at the 10th cycle and (c) cycling performance of the FTC-GO and TC-GO electrodes at 0.15 mA/cm^2 for the first cycle and 0.3 mA/cm^2 for the following cycles. The polysulfide catholyte is composed of 1 M LiTFSI, 0.1 M $LiNO_3$ and 0.4 M Li_2S_6 in DOL/DME (1:1, *v*/*v*). (Sulfur loading: ~1.8 mgS in catholyte per cm^2 of the GO electrodes)

SCHEMES

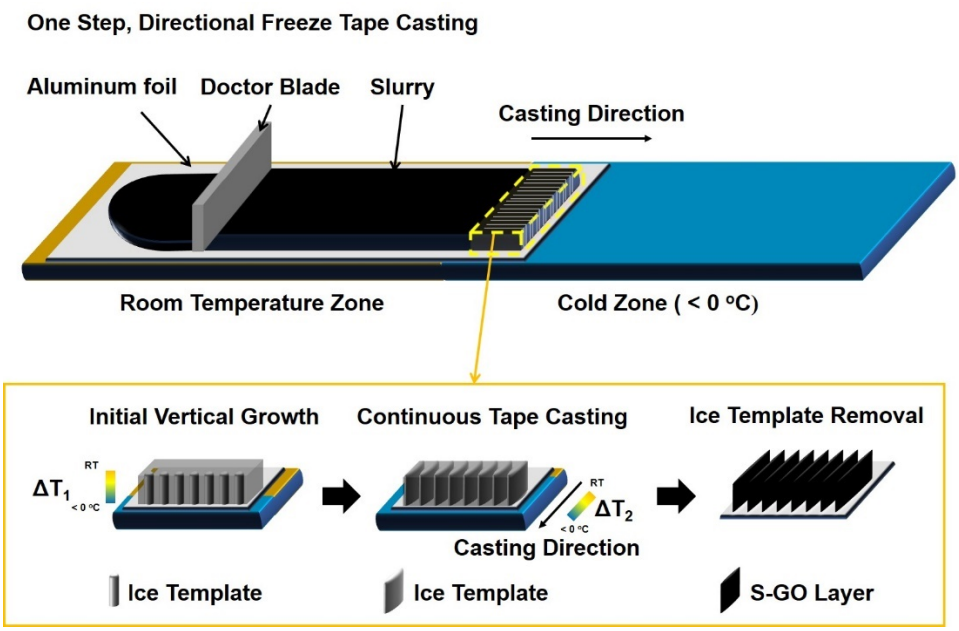

Scheme 1. Schematic illustration of the freeze tape casting process.

ASSOCIATED CONTENT

Supporting Information.

The following files are available free of charge.

Experimental method, SEM, TGA, Fourier transform pattern, Micro CT image, Voltage profile, Cycle performance, Polysulfide test results, UV-vis test results (PDF)

AUTHOR INFORMATION

Corresponding Author

* Elton J. Cairns, ejcairns@lbl.gov

* Marca M. Doeff, mmdoeff@lbl.gov

Author Contributions

The manuscript was written through contributions of all authors. All authors have given approval to the final version of the manuscript. ‡These authors contributed equally. Y. H. synthesized the S-GO-CTA composites and performed TGA, polysulfide absorption tests, SEM and electrochemical techniques. E. Y. conducted the freeze tape casting. Y. H, H. S. and D. Y. P. performed X-ray CT. H. S., J. K. and K. C. performed interlayer spacing calculations and imaging processing along with FFT. Y. S. conducted UV-vis. Y. H. and E. Y. authored the first manuscript draft. E. J. C. and M. M. D. provided constructive advice for experiments and revised the manuscript. All authors discussed the results and contributed to preparing the manuscript.

ACKNOWLEDGMENT

This work was supported by the Assistant Secretary for Energy Efficiency and Renewable Energy, Office of Vehicle Technologies of the U.S. Department of Energy under Contract No. DE-AC02-05CH11231. We thank Tevye Kuykendall and the Molecular Foundry at the Lawrence Berkeley National Laboratory for use of the scanning electron microscope. Work at the Molecular Foundry was supported by the Office of Science, Office of Basic Energy Sciences, of the U.S. Department of Energy under Contract No. DE-AC02-05CH11231. Micro X-ray CT (beamline 8.3.2) was performed at the Advanced Light Source, which is supported by the Director, Office of Science, Office of Basic Energy Sciences, of the U.S. Department of Energy under Contract No. DE-AC02-05CH11231.

REFERENCES

1. Bruce, P. G.; Freunberger, S. A.; Hardwick, L. J.; Tarascon, J.-M. *Nat. Mater.* **2011,** 11, 19-29.

2. Ji, X.; Nazar, L. F. *J. Mater. Chem.* **2010,** 20, 9821-9826.

3. Yang, Y.; Zheng, G.; Cui, Y. *Chem. Soc. Rev.* **2013,** 42, 3018-3032.

4. Yamin, H.; Peled, E. *J. Power Sources* **1983,** 9, 281-287.

5. Mikhaylik, Y. V.; Akridge, J. R. *J. Electrochem. Soc.* **2004,** 151, A1969-A1976.

6. Zheng, D.; Wang, G.; Liu, D.; Si, J.; Ding, T.; Qu, D.; Yang, X.; Qu, D. *Adv. Mater. Tech.* **2018,** 3, 1700233.

7. Zheng, D.; Zhang, X.; Wang, J.; Qu, D.; Yang, X.; Qu, D. *J. Power Sources* **2016,** 301, 312-316.

8. Chung, S.-H.; Manthiram, A. *Joule* **2018,** 2, 710-724.

9. Peng, H.-J.; Xu, W.-T.; Zhu, L.; Wang, D.-W.; Huang, J.-Q.; Cheng, X.-B.; Yuan, Z.; Wei, F.; Zhang, Q. *Adv. Funct. Mater.* **2016,** 26, 6351-6358.

10. Hwa, Y.; Seo, H. K.; Yuk, J.-M.; Cairns, E. J. *Nano Lett.* **2017,** 17, 7086-7094.

11. Chung, S.-H.; Manthiram, A. *Adv. Mater.* **2018,** 30, 1705951.

12. Hwa, Y.; Frischmann, P. D.; Helms, B. A.; Cairns, E. J. *Chem. Mater.* **2018,** 30, 685-691.

13. Yu, B.-C.; Jung, J.-W.; Park, K.; Goodenough, J. B. *Energy Environ. Sci.* **2017,** 10, 86-90.

14. Hwang, J.-Y.; Kim, H. M.; Lee, S.-K.; Lee, J.-H.; Abouimrane, A.; Khaleel, M. A.; Belharouak, I.; Manthiram, A.; Sun, Y.-K. *Adv. Energy Mater.* **2016,** 6, 1501480.

15. Je, S. H.; Kim, H. J.; Kim, J.; Choi, J. W.; Coskun, A. *Adv. Funct. Mater.* **2017,** 27, 1703947.

16. Hwa, Y.; Zhao, J.; Cairns, E. J. *Nano Lett.* **2015,** 15, 3479-3486.

17. Liang, X.; Hart, C.; Pang, Q.; Garsuch, A.; Weiss, T.; Nazar, L. F. *Nat. Commun.* **2015,** 6, 5682.

18. Wang, G.; Zheng, D.; Liu, D.; Yang, X.-Q.; Qu, D. *Carbon* **2017,** 119, 460-463.

19. Scotti, K. L.; Dunand, D. C. *Prog. Mater. Sci.* **2018,** 94, 243-305.

20. Deville, S. *Adv. Eng. Mater.* **2008,** 10, 155-169.

21. Amin, R.; Delattre, B.; Tomsia, A. P.; Chiang, Y.-M. *ACS App. Energy Mater.* **2018,** 1, 4976-4981.

22. Behr, S.; Amin, R.; Chiang, Y.-M.; Tomsia, A. P. *Ceram. forum int.* **2015,** 92, E39-E43.

23. Sofie, S. W. *J. Am. Ceram. Soc.* **2007,** 90, 2024-2031.

24. Ghadkolai, M. A.; Creager, S.; Nanda, J.; Bordia, R. K. *J. Electrochem. Soc.* **2017,** 164, A2603-A2610.

25. Sander, J. S.; Erb, R. M.; Li, L.; Gurijala, A.; Chiang, Y. M. *Nat. Energy* **2016,** 1, 16099.

26. Kim, Y.; Drews, A.; Chandrasekaran, R.; Miller, T.; Sakamoto, J. *Ionics* **2018,** 24, 2935-2943.

27. Huang, C.; Grant, P. S. *J. Mater. Chem. A* **2018,** 6, 14689-14699.

28. Song, M.-K.; Zhang, Y.; Cairns, E. J. *Nano Lett.* **2013,** 13, 5891-5899.

29. Ji, L.; Rao, M.; Zheng, H.; Zhang, L.; Li, Y.; Duan, W.; Guo, J.; Cairns, E. J.; Zhang, Y. *J. Am. Chem. Soc.* **2011,** 133, 18522-18525.

TABLE of CONTENTS